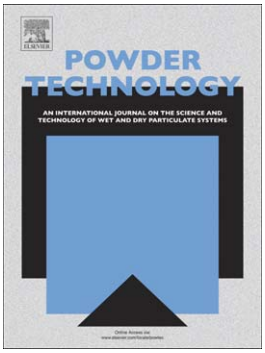

An experimental investigation of the micromechanics of Eglin sand

V Nardelli, M R Coop, J E Andrade, F Paccagnella

PII: S0032-5910(17)30126-2
DOI: doi:10.1016/j.powtec.2017.02.009
Reference: PTEC 12347

To appear in: *Powder Technology*

Received date: 6 October 2016
Revised date: 28 January 2017
Accepted date: 3 February 2017

Please cite this article as: V. Nardelli, M.R. Coop, J.E. Andrade, F. Paccagnella, An experimental investigation of the micromechanics of Eglin sand, *Powder Technology* (2017), doi:10.1016/j.powtec.2017.02.009

An experimental investigation of the micromechanics of Eglin sand

V. Nardelli*, M. R. Coop, J. E. Andrade and F. Paccagnella

*Tel.: + 852 3442 6528, email: vnardelli2-c@my.cityu.edu.hk

Abstract

The mechanical behaviour of Eglin sand at the micro-scale was studied in this work. Laboratory experiments using unconventional apparatuses were carried out in order to study the contact behaviour of pairs of particles in both compression (normal loading) and shearing (tangential loading) and the strength of grains. Particle fractions were identified according to their colour by visual observation and both their chemical composition and surface morphologies were obtained. The tangential stiffnesses and inter-particle coefficients of frictions for the different fractions found in the sand sample were determined under the range of normal loadings applied (1-9N). The results show some discrepancies between the theoretical models commonly found in literature to describe either the normal or the tangential loading response, which are able to predict the trend of the force-displacement curves but using elastic moduli that are lower than those found in literature, especially in the case of tangential loading. Also, the results of particle crushing tests show quite consistent results (excluding one particle group), probably related to the similar mineralogy of all fractions, which are mainly constituted by silica.

Keywords: sands; stiffness; friction; particle strength

1. Introduction

The behaviour of granular materials regarded as discrete elements has been gaining acceptance and popularity since the work by Cundall and Strack [1] with the use of numerical tools to predict their mechanical response. Many researchers have developed new methodologies in order to include more factors and variables to make their numerical analyses closer to real problems, for both quasi-static [2] or dynamic conditions, such as the case of impact of aggregates [3], including sample scale effects [4], breakage of aggregates [5] **and more complex particle shapes, such as superquadric particles [6]** and irregular particle shapes [7].

Previous experimental work has also investigated some of the main aspects related to the behaviour of sand particles at the micro-scale, in relationship with either breakage [8-10] or the contact mechanics [11-14]. Although there have been individual investigations of particle strengths in some sands and more recently some aspects of contact mechanics in others, more complete characterisations of various aspects of the micromechanics of one sand, including the differences between different particle types within that sand, have yet to be performed and that is the aim of this research. Another novel aspect of the current work is the investigation of the micro-contact mechanics of smaller sand particles than previously tested [13], which are more representative of commonly encountered sands. **Also, the contact mechanics of particles have been studied by means of numerical analyses, using the Finite Element Method to predict the contact response of viscoelastic bodies in contact [15] or a viscoelastic sphere and a rigid wall [16].**

The sand investigated is a coarser fraction of the Eglin sand (particle diameter 0.8-1.8mm), which is commercially available as Quikrete Coarse Sand 1963 and is quarried in Pensacola, Florida. This is the smallest particle size that could **be** feasibly tested in the apparatus

described in this paper. Luo et al. [17] studied the dynamic compressive behaviour of a finer fraction of Eglin sand under very high confinement using a long split Hopkinson pressure bar at high strain rates for constitutive modelling and mesoscale simulations. Martin and Cazacu [18] investigated the mechanical behaviour of Eglin sand up to high pressures in the triaxial cell, studying its creep behaviour and developing a model based on their experimental results. Wang et al. [19] performed nanoindentation tests also on a finer fraction of Eglin sand, in order to study the behaviour of this material as ballistic protection for military structures. They determined a Young's modulus of 72.4±2.8GPa and a hardness of 11.2±0.7GPa for a particle diameter around 0.7mm, although they did not distinguish between particle types as has been suggested here. **Cole [14] performed shear and compression tests on particle pairs of Eglin sand by means of an experimental device applying sinusoidally varying shear forces or ramp tests, measuring coefficients of inter-particle friction of 25.6±12.4° for confining loads between 1 and 5N and 28.4±4° for confining loads between 7.5 and 10N during the shear tests.**

Senatore et al. [20] used the Quikrete Medium Sand 1962 in order to study and predict the performance of lightweight vehicles for aerospace engineering purposes, comparing for this material with those obtained for the Mojave Martian simulant. These kinds of investigations are carried out by means of experiments using special test rigs [21-22], while the behaviour of vehicles over granular materials has been studied also through numerical tools, for example using the Discrete Element Method [23-24]. The Quikrete Medium Sand is slightly finer than that used in this work, but would be not possible to use in the contact micromechanics investigation described in this paper. However, given the similarity of geological origin it is believed that this investigation should be applicable also to those described previously.

2. Experimental equipment

The contact tests between pairs of particles have been carried out by means of the Inter-Particle Loading Apparatus, which is a custom-made device designed and built at the City University of Hong Kong [25]. The device has been recently upgraded and its current configuration is capable of applying combinations of either forces or displacement along three orthogonal directions [26]. Other important upgrades include the improvement of the accuracy of the displacement measurements and the increase of the apparatus' stiffness, which also improves the accuracy and reliability of the measured displacements.

The apparatus consists of a stainless steel loading frame, three loading arms and a stainless steel sled (Fig.1). Each loading arm is assembled connecting a micro linear actuator (a) and a load cell (b) by means of stiff mechanical parts. The vertical loading arm is connected to the loading frame, while the two horizontal ones are orientated along two orthogonal directions and are mounted on a stainless steel base. The two horizontal loading arms are also connected to the sled (c) by means of a special connection built using two orthogonal linear bearings. The end of the vertical arm and the sled are both equipped with wells that are used to mount brass holders with the two sand particles on their top (d). The particles were glued to the brass particle holders by means of super glue prior to being tested, waiting at least 24 hours to guarantee the hardening of the glue. The two particles were then gently brought into contact prior to being tested. Two digital micro-cameras (e) are used to determine and control the precise location and orientation of the contact area between the two sand particles and to record images during each test.

The displacements are measured by means of eddy-current non-contact displacement sensors (f) that have a resolution of 10^{-5}mm and a measuring range of 3mm. The two horizontal

transducers are mounted on the sled, in order to minimise any compliance effects of the apparatus. A low-pass filter has been built in order to ensure the highest possible resolution for the displacement measurements. The loads are measured using high-resolution load cells having a capacity of 100N. The vertical load cell is of a particularly stiff design, again to minimise compliance, which might influence the application of the horizontal loads.

The whole apparatus is placed inside a Perspex chamber, in order to carry out the tests while varying the environmental conditions. These are controlled using a humidity controller that enables the control of the relative humidity inside the chamber within the range 15-85%. Also, tests using a small bath around the particles can be carried out in order to study the influence of fluids on the contact behaviour.

The strength of Eglin sand grains have been studied by means of single-particle compression tests carried out by means of a custom-modified CBR apparatus at the City University of Hong Kong. More details about this device can be found in [10]. This apparatus consists of a loading machine, a stiff loading frame, a load cell and an LVDT for the displacement measurements. Each test was carried out compressing a single particle between two loading platens until its failure occurred.

3. Material properties and procedures

The Eglin sand sample tested is commercially available as the Quikrete Coarse Sand 1963 (Fig. 2), a commercial material that is consistently graded, washed and kiln dried prior to be commercialised. This material consists of silica grains that are mainly characterised by five different colour groups: white, black, pink-yellow (later named as pink only), grey and transparent. Table 1 shows **the results** of the chemical characterisation that was carried out

by means of the Energy-Dispersive X-ray Spectroscopy (EDS). **This procedure should be appropriate to characterise the chemical composition of the particles since each of them seemed to be constituted of a homogeneous material. Also, the mechanical tests carried out to characterise their contact behaviour involve only small portions of the particle surface and not their bulk. The analyses were repeated on several particles of each colour, confirming that colour was a suitable basis for selecting the particles because the data were consistent. Average values are given in Table 1.** It can be observed that all the grain types are mainly constituted of silicon and oxygen. The white particles should be identified as feldspar (i.e. anorthoclase), while the transparent fraction appears to include both feldspar (i.e. orthoclase) and quartz particles, which seem difficult to identify by visual observation only. The black, grey and pink particles show more complex compositions, where potassium, sodium, magnesium and fluorine coexist along with the silicon, oxygen, aluminium and iron that are the main components of most of the particles. The black particles also include calcium and manganese fractions, while the pink particles contain small traces of calcium and titanium. The black particles were identified as hornblende, while from their complex composition those that are grey and pink should be fragments of igneous rocks such as granite and rhyolite.

The particles were examined before testing, measuring their diameters along three orthogonal directions and estimating their shape parameters, roundness and sphericity, by means of visual observation using the Krumbein and Sloss chart [27]. The sphericity quantifies the similarity of the overall shape of a particle to a sphere, higher numbers being more spherical, while the roundness quantifies the sharpness of edges and corners, low values being more angular or less rounded. Table 2 illustrates the average values of diameter, roundness and sphericity for the five groups of particles that were identified according to their colour. These

data were obtained for all the particles that were tested, hence over 200 particles were examined.

The RMS roughness (S_q) of a small number of particles was investigated through white light interferometry and the average values for each group are included in Table 2. An average overall value of about 0.53μm was determined over areas around of 30x30μm. The exceptions are the pink particles which are significantly less rough and the grey particles, for which areas of 16x16μm had to be used because of difficulties related to the interferometry images of these. Generally, a smaller area should lead to a smaller roughness and so this probably means that the grey particles are slightly rougher. Figure 3 shows an image of the particle surface morphology of a black particle taken using the interferometer over a larger area of 106x106μm. The RMS roughness measured for this particle is 1.21μm over the whole area. These values of roughness are calculated by the software which subtracts the influence of the overall shape of the particle. The roundnesses are all fairly similar, with only the grey and pink particles being slightly less angular. Although there is some variability in roughness, the values are fairly similar for the five groups as they could potentially vary over an order of magnitude. It is therefore the differences in sphericity that are probably the most significant.

Figure 4 shows SEM images of the particles and the details of their micro-surfaces using two different magnifications for each. Different particle outlines can be detected, observing that all of them exhibit some sharp edges, which is also related to the similar roundnesses shown in Table 2. **SEM images of the white particles are not included as they are characterised by an appearance that is very similar to that of transparent particles. The transparent, white and grey particles are characterised by a crystalline nature, which is also reflected by the sharp edges at the micro-scale observed in the SEM images, while the black and pink particles have an amorphous appearance.** The high-magnification SEM pictures

show irregular particle morphologies for all the different minerals that can be related to the fairly similar roughnesses in Table 2.

4. Results

The laboratory tests were carried out in order to study both the normal and tangential loading response of pairs of particles at their contacts by means of the inter-particle loading apparatus along with particle strength using a simple compression apparatus. The normal loading tests were carried out compressing the particles at their contact along the vertical direction with no horizontal force, controlling the vertical displacement rate. The tangential loading tests were performed after reaching the normal load required and keeping it constant, shearing the particles at their contact along a linear horizontal path controlling the tangential displacement rate. All the test displacements were corrected for the compliance (i.e. flexibility) of the apparatus. Around 40 tangential loading tests were carried out. All the inter-particle contact tests presented here were carried out at relative humidity around 80% and temperatures 23-25°C inside the Perspex chamber, which were controlled and monitored by means of the humidity controller, respectively.

The particle crushing tests were performed loading each single grain until breakage. A displacement rate of is 0.1mm/min was used, which was the minimum allowed by the apparatus. Around 170 tests were carried out, more than 30 for each type of mineral.

4.1 Normal loading

Figure 5 shows the compression curves for pairs of particles having different colours. **For some colours more than one test was conducted.** Some of the grain pairs were loaded up to

5N and others up to 9N. All the pairs of particles were compressed using a displacement rate of 0.1mm/h. Qualitatively, these curves show the non-linear behaviour that is expected in compression for spherical or hemispherical bodies in contact following the Hertz theory [28], with some exceptions for some grains of the pink and grey types that exhibit brittle behaviour within the area of contact and a consequent **drop of normal force after the occurrence of some breakage phenomena at the contact between the pairs of particles tested**. The results exhibit some scatter and the stiffnesses **of the curves** are not clearly related to the different mineralogies **determined for each fraction**.

Figure 6 shows the compression curves up to 9N previously given in Figure 1 along with two curves plotted using the Hertz theory of contact [28], where these curves overlap the experimental results for the stiffest (white) and the softest (transparent) pairs of particles. **The theoretical curves were plotted using a radius R=0.7mm, which corresponds to the average of all the particles tested, a Poisson's ratio ν=0.1 and Young's moduli of 94GPa and 52GPa for the stiffest and the softest curves, respectively. It should be noted that the theoretical curves plotted in Figure 6 correspond to particles (white and transparent) made either of feldspars or quartz, whose elastic parameters are E=40.5-68GPa and ν=0.32 and E=94-98GPa and ν=0.065-0.068, respectively [29].** The softest curve was plotted with an offset of 0.6μm in order to fit the relative experimental curve. **It can be observed that the theoretical model is able to describe the trend of the curves using Young's moduli similar to those found in literature, but it is not able to reproduce the initial soft part of some force-displacement curves determined experimentally.** This offset may result from the roughness of the particles at the contact as **observed by Cavarretta et al. [12] for single particle compression tests on glass ballotini and Leighton Buzzard quartz sand**, although it is very large compared to values in Table 2 and also shows no correlation with the mineral type. However, because of the limitations of

carrying out complex interferometry tests, surface roughnesses could only be determined for representative particles and not for each specific pair in contact. **Also, these offset values are characterised by a magnitude that is clearly smaller than that observed by Cavarretta et al. [12], probably because of the higher precision and resolution of the Inter-Particle Loading Apparatus compared to the device they used for their compression tests, notably in that only one contact is tested between two particles rather than taking half the displacements measured when a single particle is loaded between two steel platens.**

4.2 Tangential loading

The tangential loading tests were performed shearing the particles after applying different normal confining forces at the contact between each pair of particles. Some particles were sheared at 5N and some were sheared more than once at different load levels. These were applied following a geometric progression with common ratio 3, hence the loads applied were 1, 3 and 9N. Figures 7 and 8 show the results of all the tangential loading tests carried out at 3N in terms of force-displacement and stiffness-displacement, respectively. The stiffnesses are tangents, calculated as linear regressions over small intervals of displacement. **The force-displacement curves show a non-linear behaviour for very small displacements and a clear steady state could not be observed for large displacements for most of the particle pairs, probably because of the brittleness of the surfaces in contact which caused some evident drops of tangential force. This was observed frequently after the tests (Fig. 9).** The data show some scatter for both friction coefficients and stiffnesses, but it can be noted that the feldspathic sands (white and transparent) have similar initial tangential stiffness.

The tangential stiffness of Eglin sand does not show a well defined dependency on the normal load at the particles contact, unlike what was observed by Senetakis et al. [13] for

Leighton Buzzard quartz sand. Figures 10 and 11 illustrate the tangential test results in terms of force-displacement and stiffness-displacement, respectively, for all the black sand particles tested. The scatter of the curves is quite marked. For example, the particle pairs identified as MS9 and MS15 have stiffnesses that are completely different even if they were tested at the same load level. This suggests that the stiffnesses may depend on other properties directly related to the contact between the particles tested, perhaps roughness or local shape. The low stiffnesses of particles MS9 may be partially explained by the damage observed on their contact surface after the test.

Figures 12 and 13 show comparisons between the experimental results for a pair of white particles and one of black particles along with the corresponding theoretical predictions using the Mindlin and Deresiewicz model [30]. Two theoretical curves were plotted: one was determined using the initial tangential contact stiffness K_T following the expression:

$$K_{T,0} = 8a\left(\frac{2-\nu_1}{G_1} + \frac{2-\nu_2}{G_2}\right)^{-1} \quad (1)$$

where a is the area of contact calculated using the Hertzian expression while ν_1, ν_2 and G_1, G_2 are the Poisson's ratios and shear moduli of the two bodies in contact, the values being found in literature. Values of G=15GPa and ν=0.32 were used for the white particles (Fig. 12), which are representative of feldspar [29] while G=27.1GPa and ν=0.25 were used to model the behaviour of the black particles (Fig. 13) as they were identified as hornblende [27]. The other theoretical curve was plotted using the initial stiffness determined experimentally. The agreement between the experimental curves and those plotted using the M&D model with the experimental initial stiffness is quite good, especially for the feldspathic (white) particles (Fig. 12). The two figures show a poorer agreement between the experimental curves and those plotted using the M&D model with initial stiffness calculated theoretically. It should be noted that the prediction with the calculated initial stiffness of the

initial reverse shearing curve is very close to that obtained experimentally, with a larger divergence afterwards. Also, the overall agreement between the experimental and the theoretical curves seems to be better for the black particles (Fig. 13). **These discrepancies between the theoretical curves and the models can be ascribed to the rôle of particle roughness and its influence on the calculation of the area of contact between the two particles, the rôle of hardness of the particles surfaces and the complexity of particle geometry and their surfaces compared with that of homogeneous smooth spherical bodies, which is one of the main hypotheses of the theoretical M&D model. Another possible aspect that influences the contact behaviour of particles is their local radius of curvature at the contact location, which cannot be determined easily.**

Figure 14 illustrates the failure envelopes for each different mineral identified in the sand sample. There is again significant variability of the data, but it is evident that the white (feldspar) and transparent (feldspar and quartz) particles exhibit the higher friction coefficients, followed by the grey, black and pink particles. The lower values determined for these minerals might be explained by the observation of wear or surface damage on the surface of these particles after the tests, especially at higher normal confinements. Generally, an increase of the friction coefficient seems to follow an increase of roughness, with the exception of the grey particles. The overall mean inter-particle friction angle for all the pairs of particles is equal to 17.7±6.9° while the overall value obtained excluding those particles that were damaged during the tests is 19.1±5.7°. **These values and their scatters are lower than those determined for Eglin sand by Cole [14], although his tests were carried out on pairs of particles from different mineral fractions, which probably added some more variability in the test results.**

4.3 Particle crushing

The survival probabilities of grain crushing for each kind of mineral are plotted along with the characteristic stress in Figure 15, following the work of Nakata et al. [9]. The stresses have been determined over an ideal elliptical area calculated using the minimum and the intermediate diameters of each particle [10, 32], which have been measured using a digital calliper that has an accuracy of ±0.01mm. These curves have been obtained from the results of thirty particle crushing tests for each type of mineral. The failure stresses at 37% survival probability calculated for all the different minerals appear quite consistent (grey: 21MPa, white: 28MPa, pink: 30MPa, black: 36MPa), apart from that for the transparent particles, which is much higher at about 64MPa, which might be influenced by the higher strength of the quartz particles that can be found in this fraction. The m-moduli have been determined for each mineral and are shown in Figure 16. These represent a measure of the variability in strength in Weibull statistics [33]. The graphs shows the consistency of the m-moduli for all the different sand minerals, where most of the values are included in the interval between 2 and 3. Some scatter can be observed for the values corresponding to the maximum and minimum crushing probabilities, but otherwise the variability of strength is similar for the various minerals, despite the different strength of the transparent particles.

5. Conclusions

An experimental investigation of the micromechanics of the Eglin sand has been presented. The EDS showed that the sample seems to be made of different components, which corresponded to their colour and were feldspars, quartz, hornblende, and particles derived from granite and rhyolite.

The normal loading tests showed some variability but that the results can be fitted by the theoretical curves plotted using the Hertz' theory [28] using Young's moduli between 52 and 94GPa, which are values close to those determined from nanoindentation tests (72.4GPa) [19]. The tangential loading tests also showed some scatter in terms of stiffness and friction coefficient, probably related to wear and damage of particles during the tests, as observed after removing the particles from the apparatus. The experimental results agreed poorly with the Mindlin and Deresiewicz model [30] when the expression to calculate the initial tangential stiffness was used, while the theoretical curves plotted using the stiffness determined experimentally seem to fit more accurately. The average inter-particle friction angles vary between 14.0° and 20.4°, which are significantly larger than those determined for Leighton Buzzard Sand (9.9°) [34]. This may be related to the higher surface roughnesses measured for the Eglin sand compared with LBS (0.38±0.19μm). Even if the main component for both the two sands is silica, the more detailed analysis of the composition of the Eglin sand has revealed a more complex mineralogy.

The particle crushing tests showed the consistency of the failure stresses for all the different minerals tested, while higher values were observed for the transparent particles, probably because of the predominant presence of stronger quartz particles in this fraction. Also, the m-moduli determined for all the minerals are mainly within the range between 2 to 3, which are not far from those determined for quartz and feldspathic particles [9] of similar diameters.

The key limitations of the work were firstly that these tests were conducted at the lower limit of particle size that could be used in the apparatus that had previously tested only particles with an average diameter of 2mm. The smallest load at which shearing could be conducted with accurate control was therefore only 1N. The load levels in strong

force chains are highly variable [35] but for such small particles it would have been desirable also to test with some smaller loads, although the typical loads used in Atomic Force Microscope friction tests [36] are far too small to be representative. The other key limitation is that a better understanding of the load-deflection behaviour might be obtained if the local contact geometry could be measured during the test, but techniques able to do this have yet to be developed.

Acknowledgments

The authors would like to thank Prof. G. Viggiani and Dr E. Andó of the Laboratoire 3S-R of Grenoble, France, for supplying the sand tested in this work. They also thank Dr B. Baudet for the use of the interferometer at the University of Hong Kong. The technicians of City University of Hong Kong, Mr Y.H. Tsang and Mr C.K. Lai are acknowledged for their technical help. This work was fully supported by a grant from the Research Grants Council of the Hong Kong Special Administrative Region, China (Project No. CityU 112712).

References

[1] P.A. Cundall, O.D.L Strack, A discrete numerical model for granular assemblies, Géotechnique 29 (1979) 47–65.

[2] C. Thornton, Numerical simulations of deviatoric shear deformation of granular media, Géotechnique 50 (2000) 43–53.

[3] K.D. Kafui, C. Thornton, Numerical simulations of impact breakage of a spherical crystalline agglomerate, Powder Technology 109 (2000) 113-132.

[4] J. Wang, M. Gutierrez, Discrete element simulations of direct shear specimen scale effects, Géotechnique 60 (2010) 395–409.

[5] C. Thornton, L. Liu, How do agglomerates break?, Powder Technology 143-144 (2004) 110-116.

[6] A. Podlozhnyuk, S. Pirker, C. Kloss, Efficient implementation of superquadric particles in Discrete Element Method within an open-source framework, Comp. Part. Mech. (2016) 1-18.

[7] J.P. de Bono, G.R. McDowell, An insight into the yielding and normal compression of sand with irregularly shaped particles using DEM, Powder Technology 271 (2015) 270-277.

[8] G.R. McDowell, M.D. Bolton, On the micromechanics of crushable aggregates, Géotechnique 48 (1998) 667–679.

[9] Y. Nakata, A.F.L. Hyde, M. Hyodo, H. Murata, A probabilistic approach to sand crushing in the triaxial test, Géotechnique 49 (1999) 567-583.

[10] M.C. Todisco, M.R. Coop, Q. Guo, K. Senetakis, The effect of coordination number on particle crushing, Proceedings of the TC105 ISSMGE International Symposium on Geomechanics from Micro to Macro, Cambridge, UK (2015) 1063-1068.

[11] D.M. Cole, J.F. Peters, Grain-scale mechanics of geological materials and lunar simulants under normal loading, Granular Matter 10 (2008) 171-185.

[12] I. Cavarretta, M.R. Coop, C. O'Sullivan, The influence of particle characteristics on the behaviour of coarse grained soils, Géotechnique 60 (2010) 413-423.

[13] K. Senetakis, M.R. Coop, M.C. Todisco, Tangential load-deflection behaviour at the contacts of soil particles, Géotechnique Letters 3 (2013) 59-66.

[14] D.M. Cole, Laboratory observations of frictional sliding of individual contacts in geologic materials, Granular Matter 17 (2015) 95-110.

[15] Q.J. Zheng, Z.Y. Zhou, A.B. Yu, Contact forces between viscoelastic ellipsoidal particles, Powder Technology 248 (2013) 25-33.

[16] Q.J. Zheng, H.P. Zhu, A.B. Yu, Finite element analysis of the contact forces between a viscoelastic sphere and rigid plane, Powder Technology 226 (2012) 130-142.

[17] H. Luo, H. Lu, W.L. Cooper, R. Komanduri, Effect of mass density on the compressive behavior of dry sand under confinement at high strain rates, Experimental Mechanics 51 (2011) 1499-1510.

[18] B.E. Martin, O. Cazacu, Experimental and theoretical investigation of the high pressure, undrained response of a cohesionless sand, International Journal for Numerical and Analytical Methods in Geomechanics 37 (2013) 2321-2347.

[19] F. Wang, B. Fu, H. Luo, S. Staggs, R.A. Mirshams, W.L. Cooper, S.Y. Park, M.J. Kim, C. Hartley, H. Lu, Characterization of the grain-level mechanical behavior of Eglin sand by nanoindentation, Experimental Mechanics 54 (2014) 871-884.

[20] C. Senatore, P. Jayakumar, K. Iagnemma, Experimental study of lightweight track vehicle performance on dry granular materials, ASA, CSSA and SSSA International Annual Meetings, Tampa, Florida, 2013.

[21] C. Senatore, M. Wulfmeier, I. Vlahinic, J. Andrade, K. Iagnemma, Design and implementation of a particle image velocimetry method for analysis of running gear-soil interaction, Journal of Terramechanics 50 (2013) 311-326.

[22] J.Y. Wong, C. Senatore, P. Jayakumar, K. Iagnemma, Predicting mobility performance of a small, lightweight track system using the computer-aided method NTVPM, Journal of Terramechanics 61 (2015) 23-32.

[23] M.A. Knuth, J.B. Johnson, M.A. Hopkins, R.J. Sullivan, J.M. Moore, Discrete element modeling of a Mars exploration rover wheel in granular material, Journal of Terramechanics 49 (2012) 27-36.

[24] W. Smith, H. Peng, Modeling of wheel-soil interaction over rough terrain using the discrete element method, Journal of Terramechanics 50 (2013) 277-287.

[25] K. Senetakis, M.R. Coop, The development of a new micro-mechanical inter-particle loading apparatus, Geotechnical Testing Journal 37 (2014) 1028-1039.

[26] V. Nardelli, M.R. Coop, C. Vitone, S. Chen, The inter-scale behaviour of two natural scaly clays, Géotechnique Letters 6 (2016) 205-210.

[27] W.C. Krumbein, L.L Sloss, Stratigraphy and sedimentation, W. H. Freeman and Company, San Francisco, 1963.

[28] H. Hertz, Über die Berührung fester elastischer Körper, J. reine und angewandte Mathematik, 92 (1882) 156-171.

[29] G. Mavko, T. Mukerji, J. Dvorkin, The rock physics handbook: tools for seismic analysis in porous media, Cambridge University Press, 1998.

[30] R.D. Mindlin, H. Deresiewicz, Elastic spheres in contact under varying oblique forces, Journal of Applied Physics (1953) 327-343.

[31] S.P. Clark, Handbook of physical constants, Geological Society of America, Memoir 97, 1966.

[32] I. Cavarretta, The influence of particle characteristics on the engineering behaviour of granular materials, PhD thesis, Imperial College, London, 2009.

[33] W. Weibull, A statistical distribution function of wide applicability, Journal of Applied Mechanics 18 (1951) 293-297.

[34] K. Senetakis, M.R. Coop, M.C. Todisco, The inter-particle coefficient of friction at the contacts of Leighton Buzzard sand quartz minerals, Soils and Foundations 53 (2013) 746-755.

[35] D. Barreto, Numerical and experimental investigation into the behaviour of granular materials under generalised stress states, PhD thesis, Imperial College, London, 2009.

[36] Q. Li, K.S. Kim, Micromechanics of friction: effect of the nanometre-scale roughness, Proceedings of the Royal Society A 494 (2008) 1319-1343.

Vitae

Mr Vincenzo Nardelli

Mr Nardelli is currently a PhD candidate in Civil Engineering at City University of Hong Kong under the supervision of Prof. Matthew Coop. After his MSc at Politecnico di Bari where he worked on the mechanical behaviour of fissured clays through element testing, his current interests focus on the micromechanics of sands, with particular regard to the contact behaviour at the grain scale. This research is still in progress and it has been developed using a custom-made inter-particle loading apparatus was designed and built at City University of Hong Kong.

Prof. Matthew R. Coop

Professor Coop has over 30 years research experience, concentrating on the behaviour of soils and weak rocks as revealed through high quality laboratory testing. More recently his interests have turned towards the micromechanics of sand particles and their relationship to macroscopic behaviour. Following his Doctorate on the behaviour of piles in clays, he was instrumental in developing the soil element research laboratory at City University, London before moving to Imperial College in 2000, where he was promoted to Professor in 2007. In 2010 he moved to the City University of Hong Kong where he established a laboratory specialising in soil element testing and the micro-mechanics of inter-particle contacts. He recently moved to University College London.

Prof. José E. Andrade

José E. Andrade is a Professor in the Division of Engineering and Applied Science at the California Institute of Technology. Andrade joined Caltech after four years at Northwestern University as an Assistant Professor of Theoretical and Applied Mechanics. Andrade got his PhD in Civil Engineering in 2006 from Stanford University. His research interests lie in the area of computational geomechanics with application to problems at the interface of physics and mechanics to develop predictive analytical and numerical models for porous materials (e.g., soils, rocks, concrete, bone, etc.).

Mr Filippo Paccagnella

Mr Paccagnella has got his MSc at Politecnico di Milano discussing a dissertation about the micromechanical behaviour of Eglin Sand. In 2015 he spent 3 months at City University of Hong Kong working in the laboratory under the supervision of Prof Coop and Mr Nardelli and performed laboratory tests in order to study the micromechanics of Eglin sand.

FIGURES

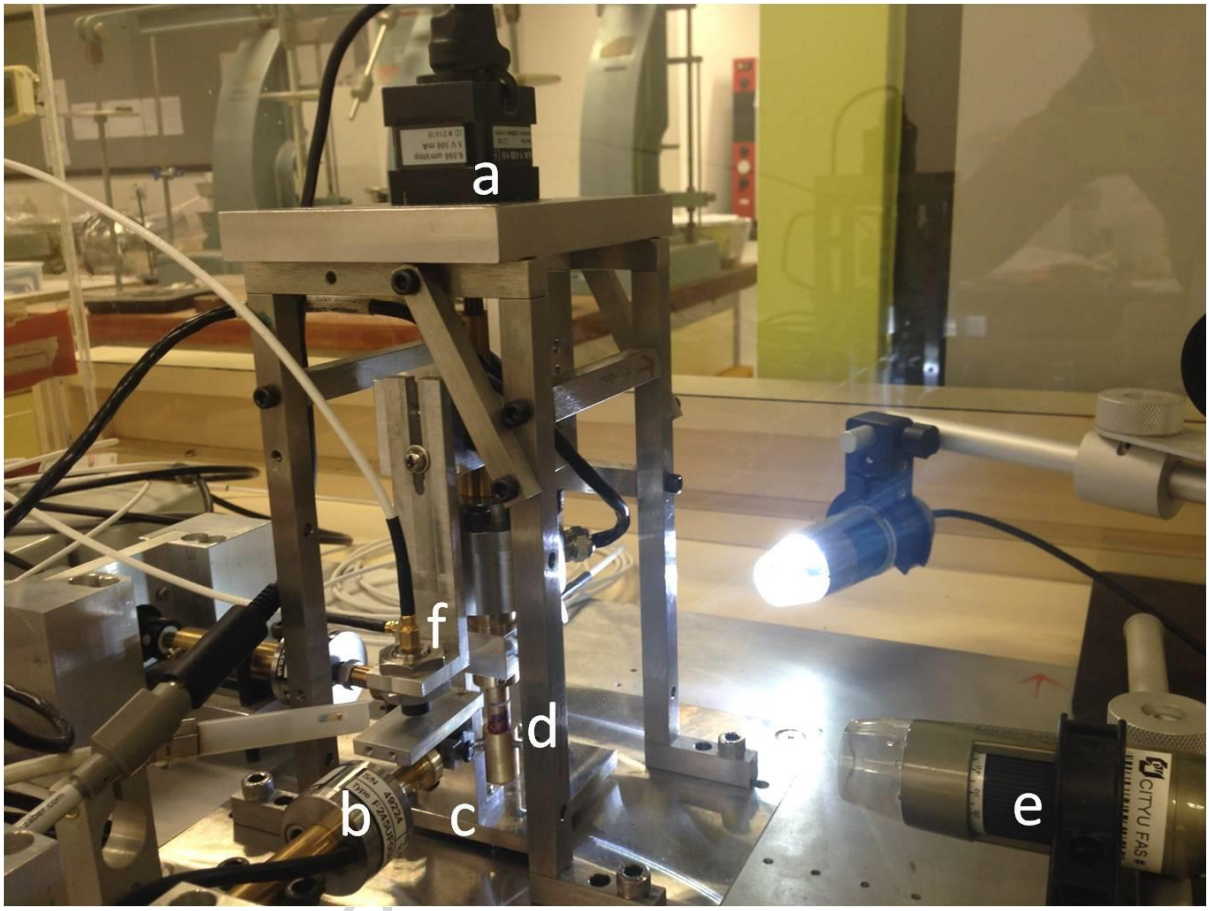

Figure 1. Inter-particle loading apparatus: a) linear actuator; b) load cell; c) stainless steel sled; d) soil particles during a test; e) digital micro-camera; f) eddy-current displacement sensor.

Figure 2. Eglin sand

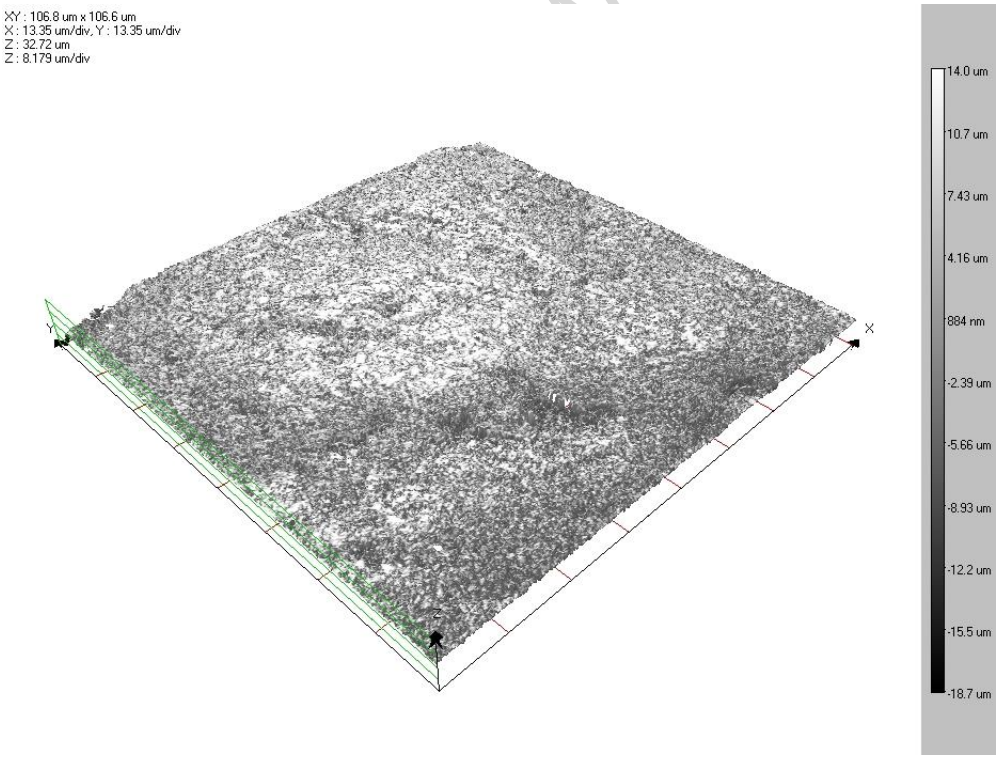

Figure 3. Surface morphology of a black particle of Eglin sand.

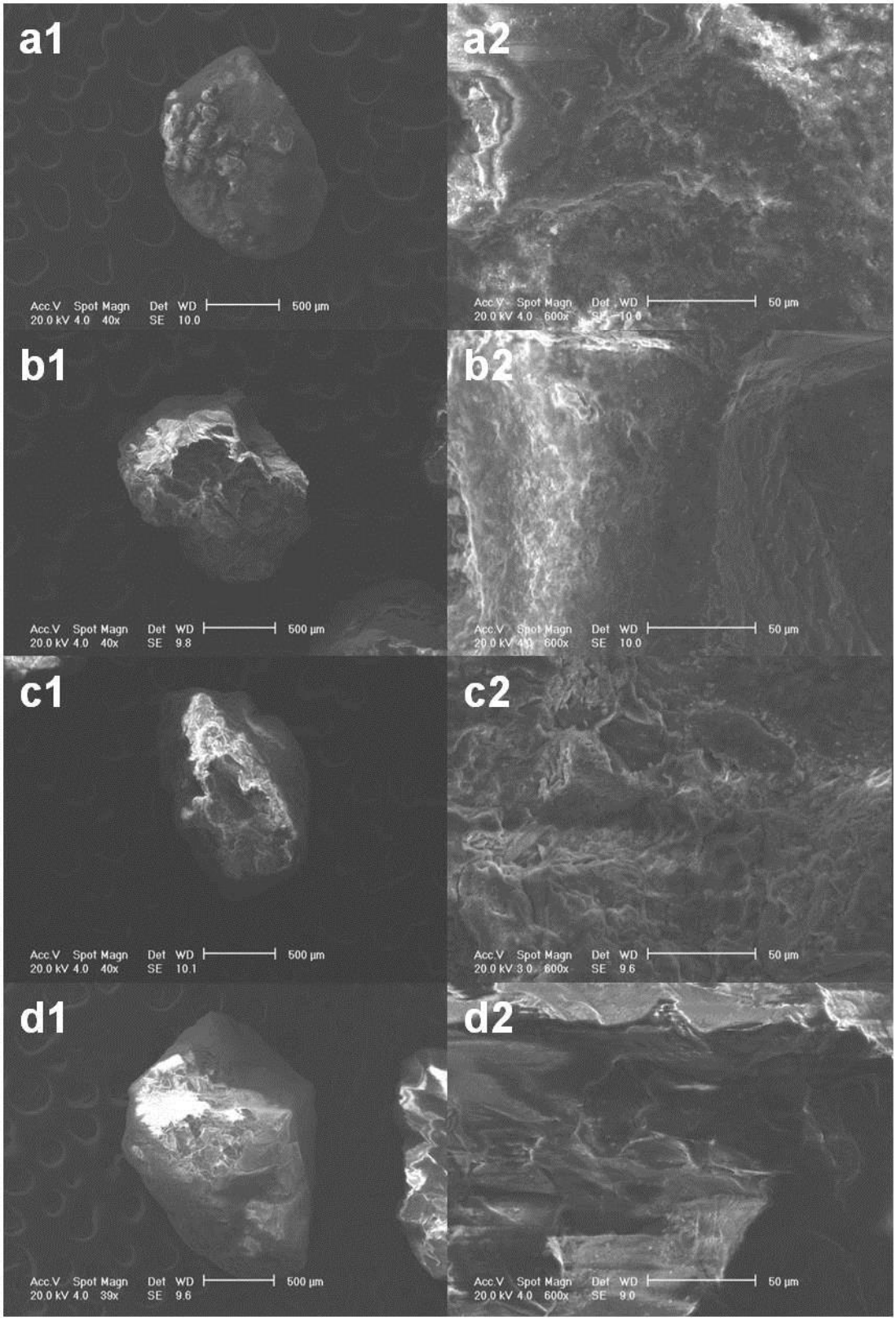

Figure 4. SEM image of Eglin sand particles: a1-2) black; b1-2) grey; c1-2) pink; d1-2) transparent.

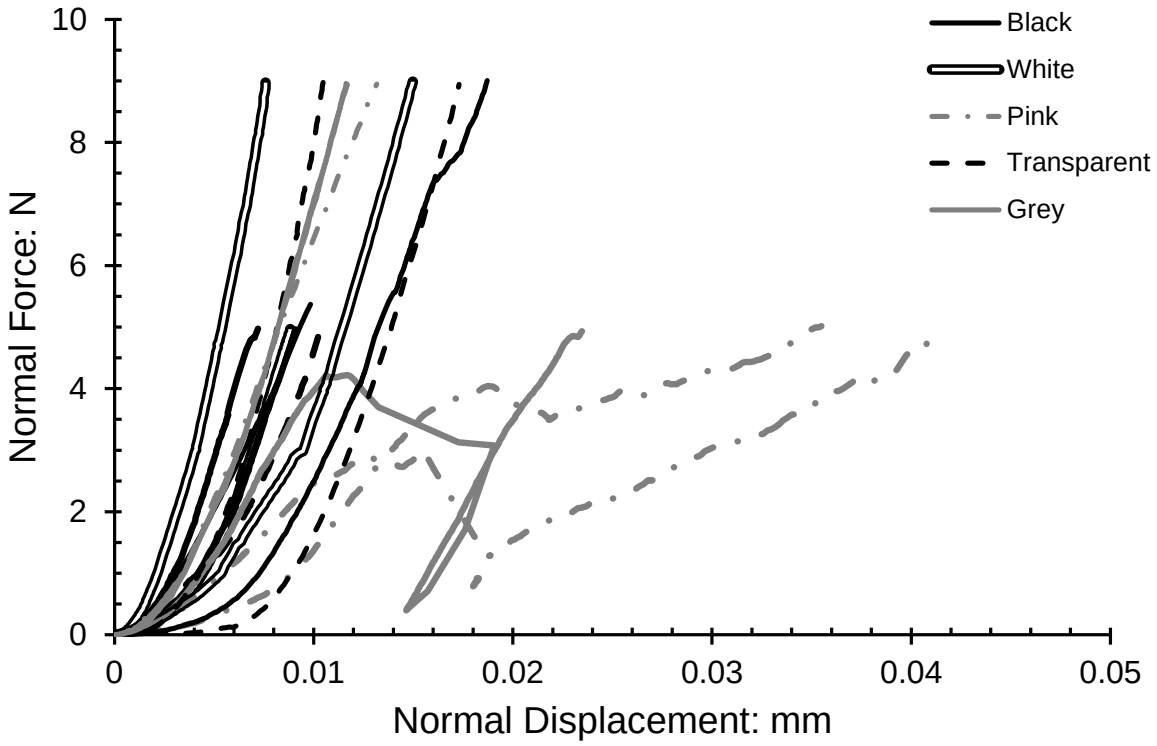

Figure 5. Normal loading test results for the Eglin sand particles.

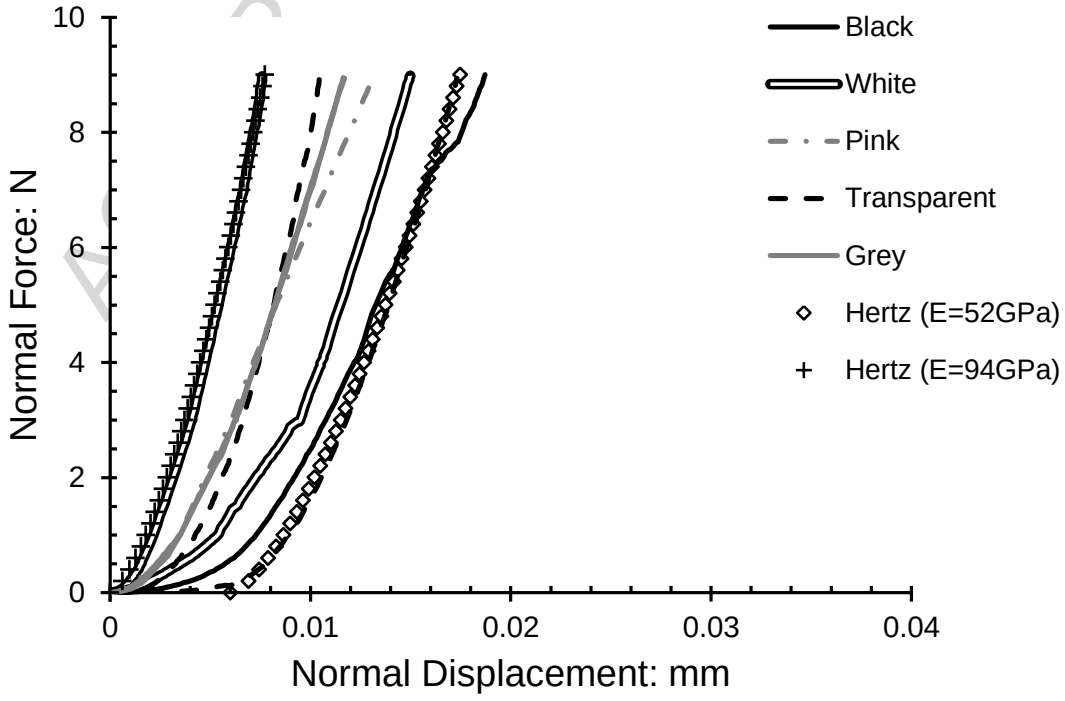

Figure 6. Normal loading test results plotted with curves obtained using Hertzian theory [28].

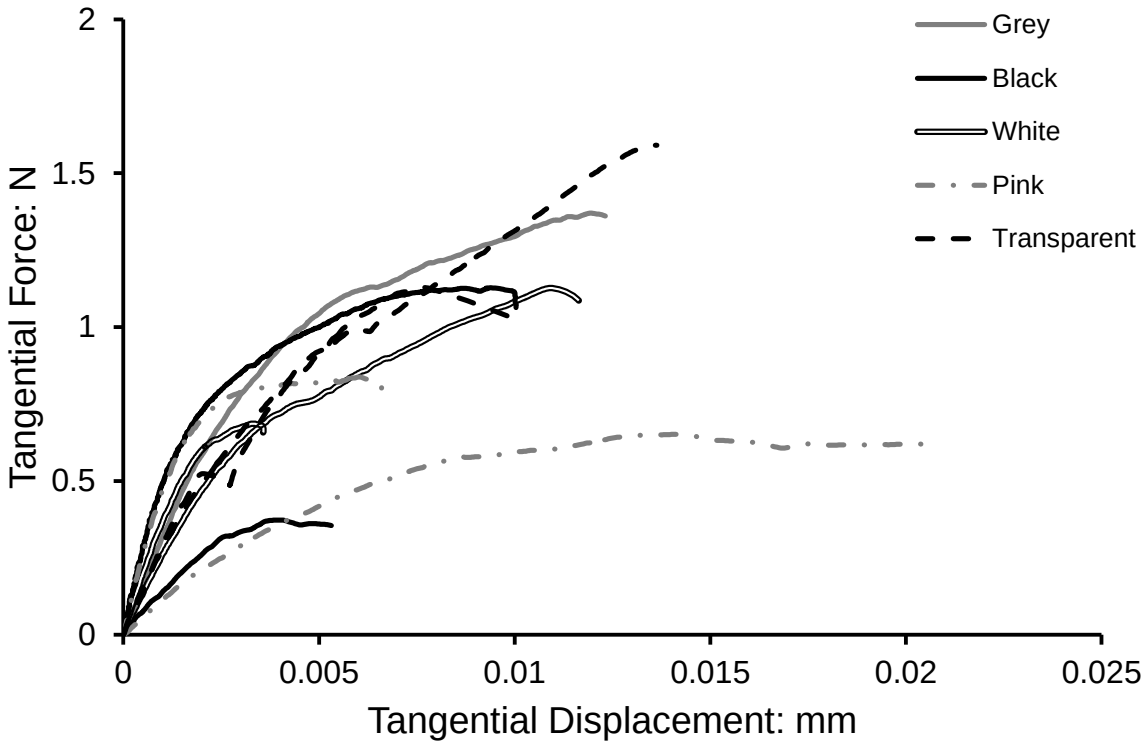

Figure 7. Tangential force-displacement curves for Eglin sand particles under a normal load of 3N.

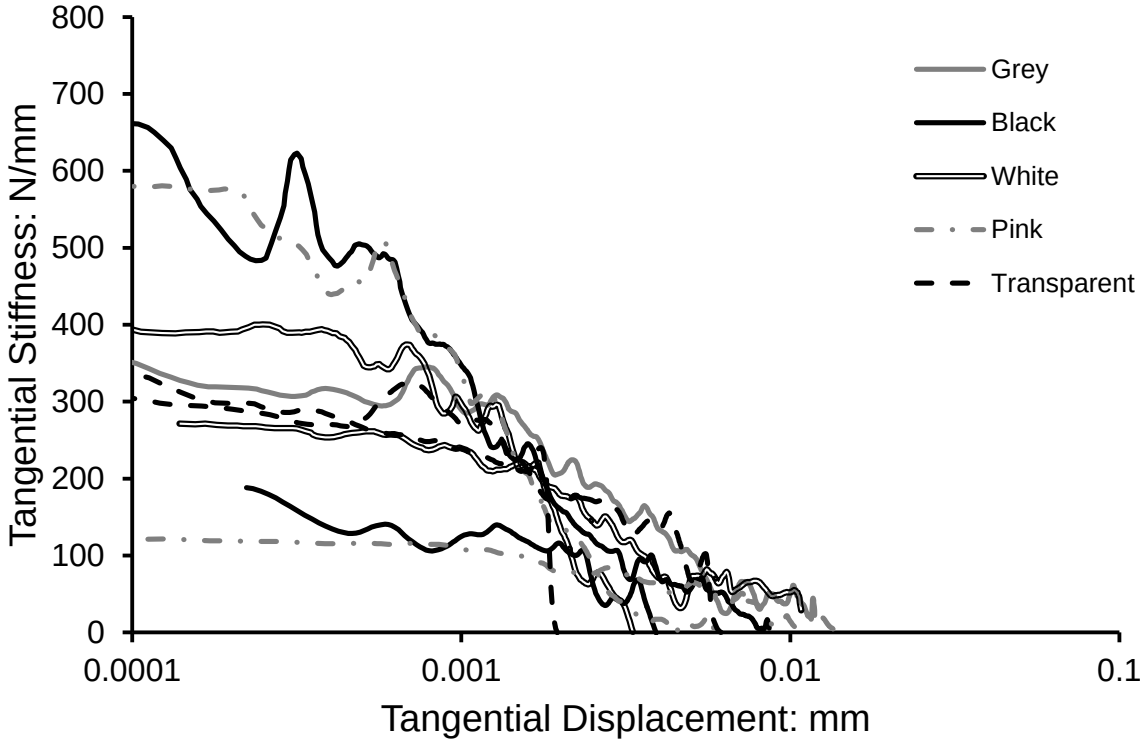

Figure 8. Tangential stiffness-displacement curves for Eglin sand particles under a normal load of 3N.

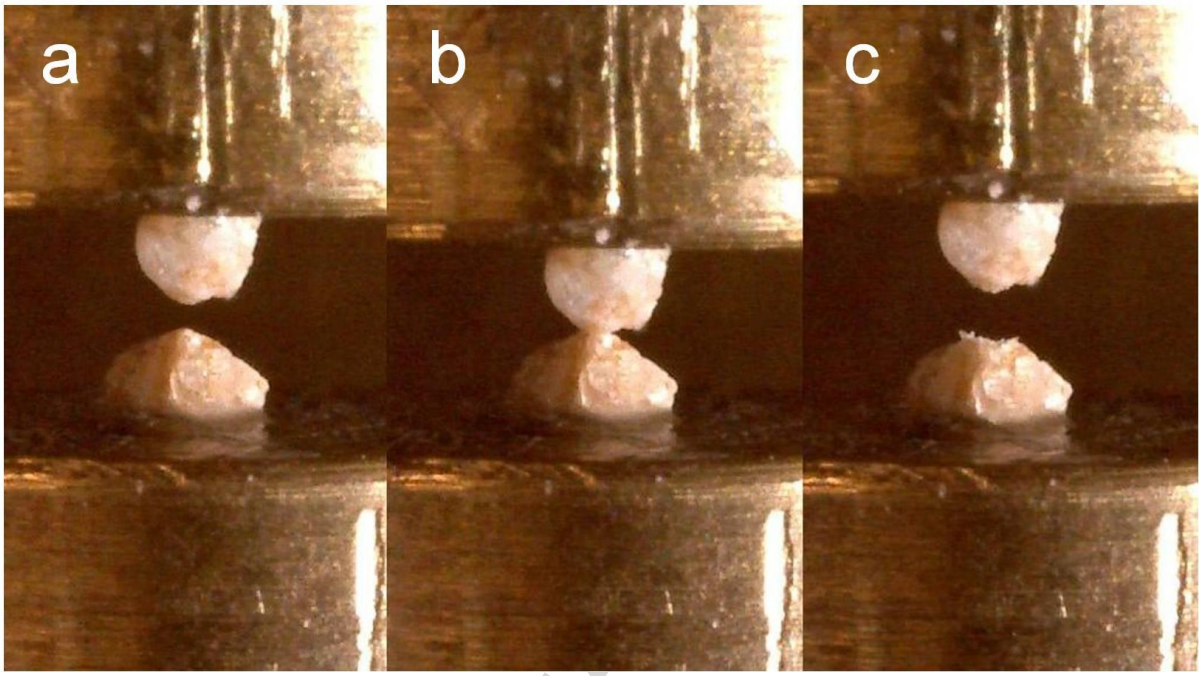

Figure 9. Pink particles of Eglin sand: a) before testing; b) during the test; c) after testing.

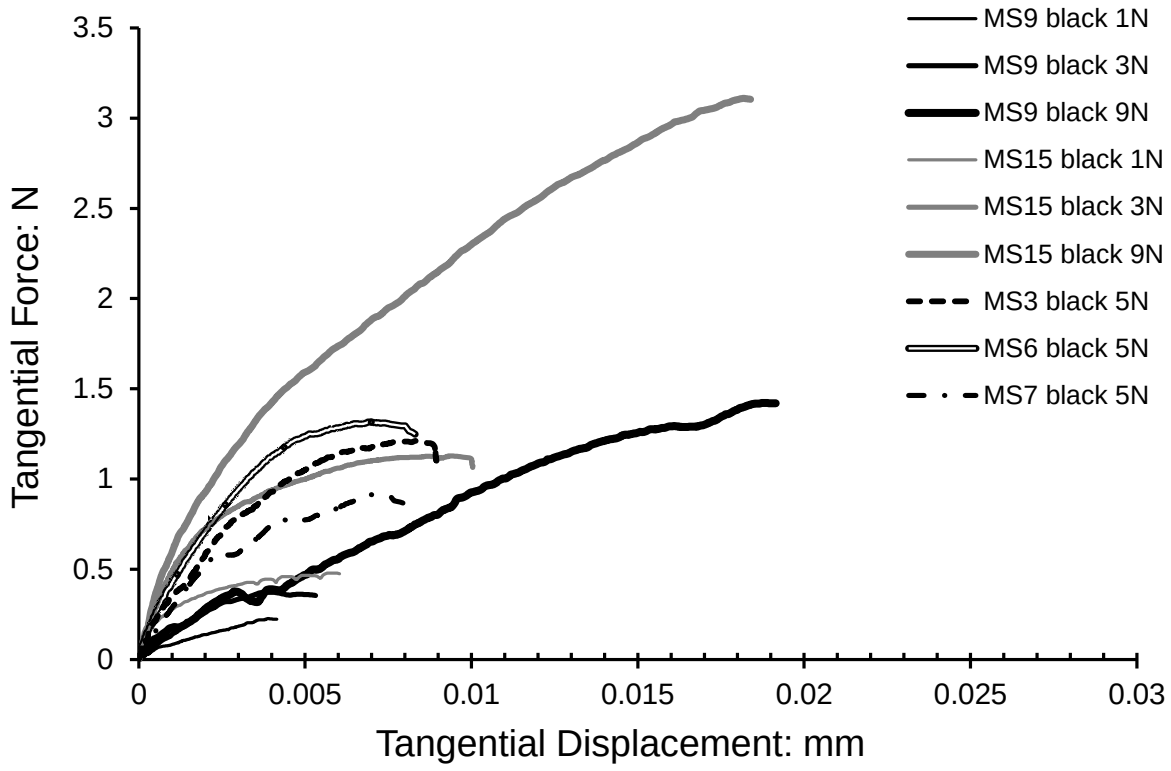

Figure 10. Tangential force-displacement curves for the black fraction of Eglin sand particles under different normal loads.

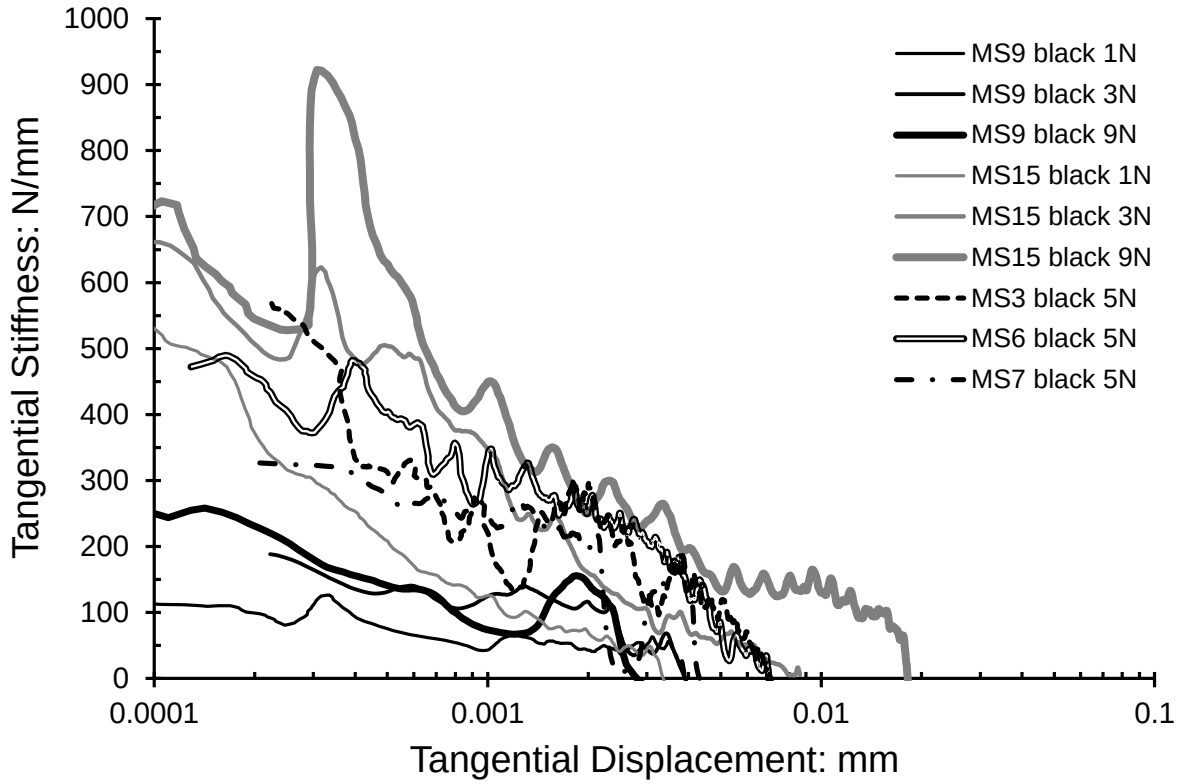

Figure 11. Tangential stiffness-displacement curves for the black fraction of Eglin sand particles under different normal loads.

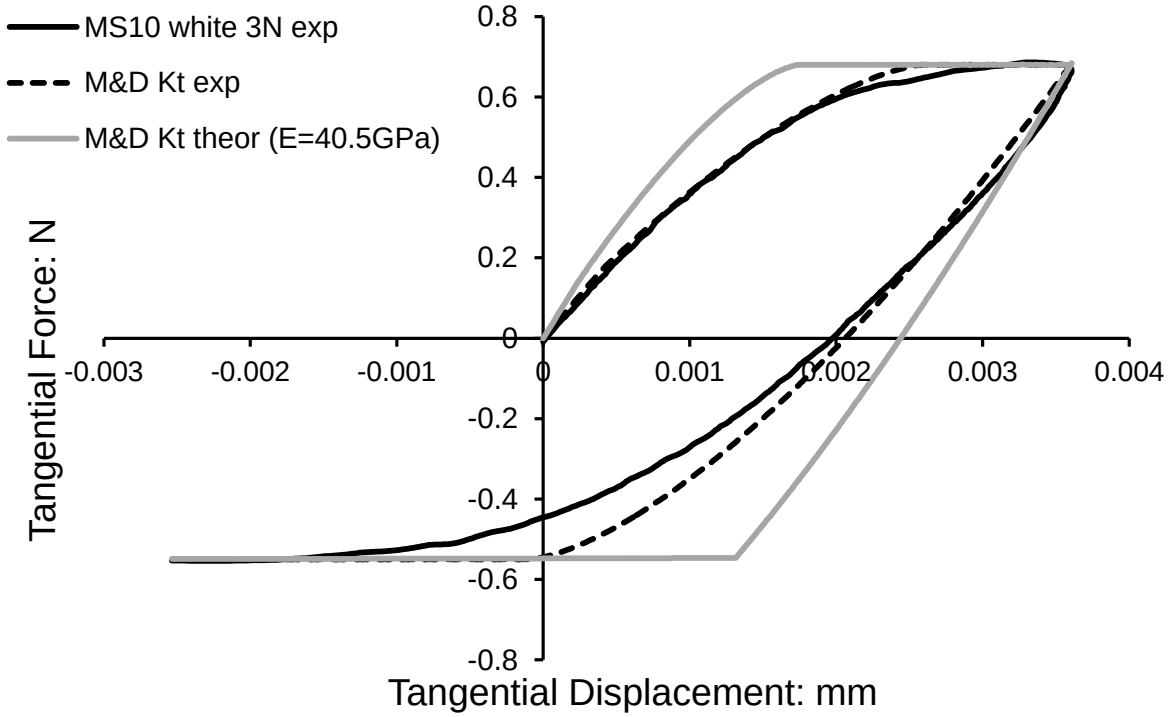

Figure 12. Comparison between the experimental curve obtained for a pair of white particles and those obtained for the Mindlin & Deresiewicz model [30] using initial stiffnesses determined theoretically and experimentally.

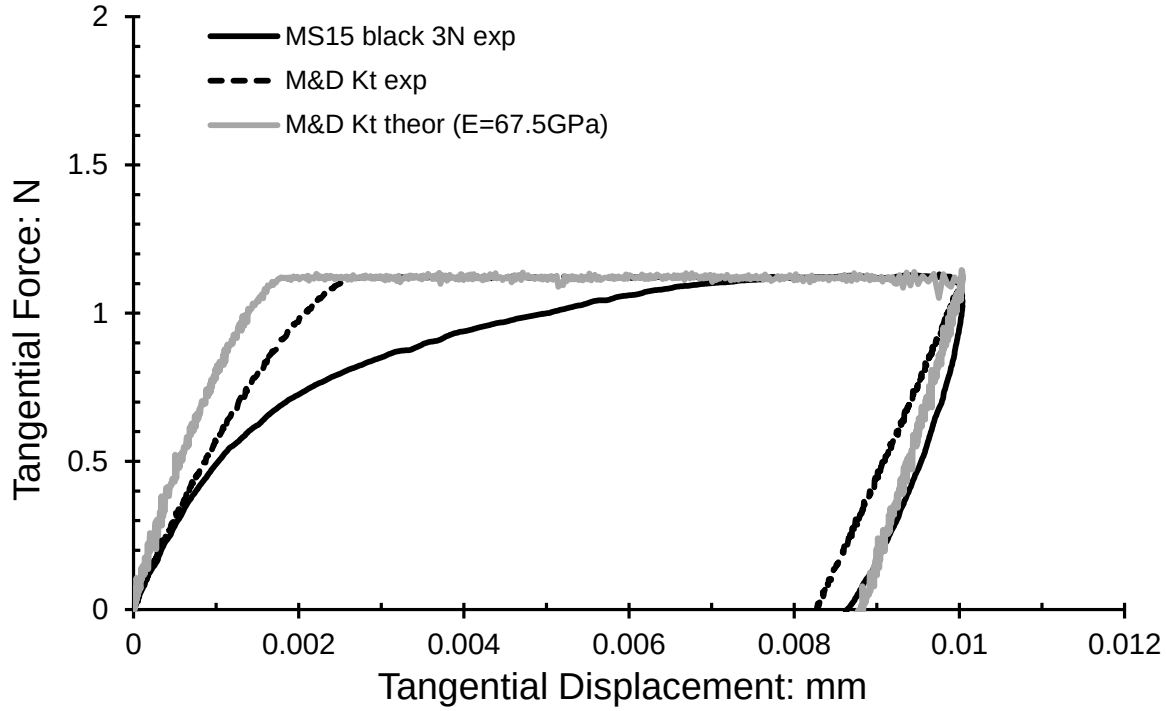

Figure 13. Comparison between the experimental curve obtained for a pair of black particles and those obtained using the Mindlin & Deresiewicz model [30] for initial stiffnesses determined theoretically and experimentally.

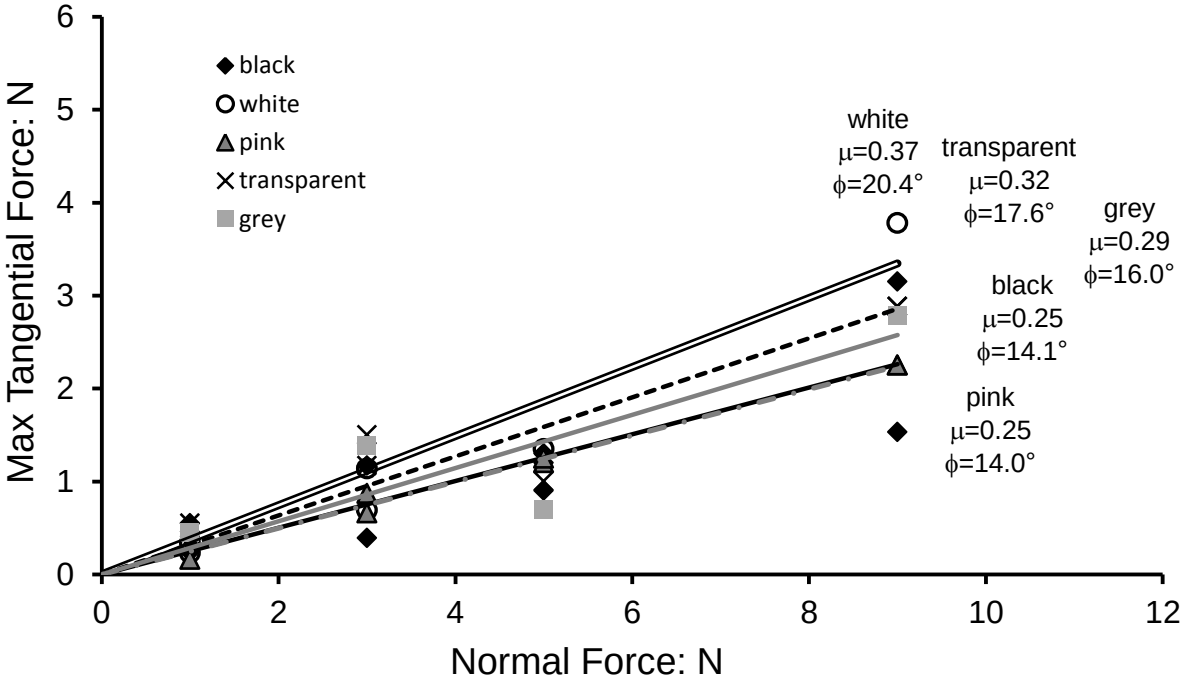

Figure 14. Failure envelopes for the different fractions identified within the Eglin sand sample.

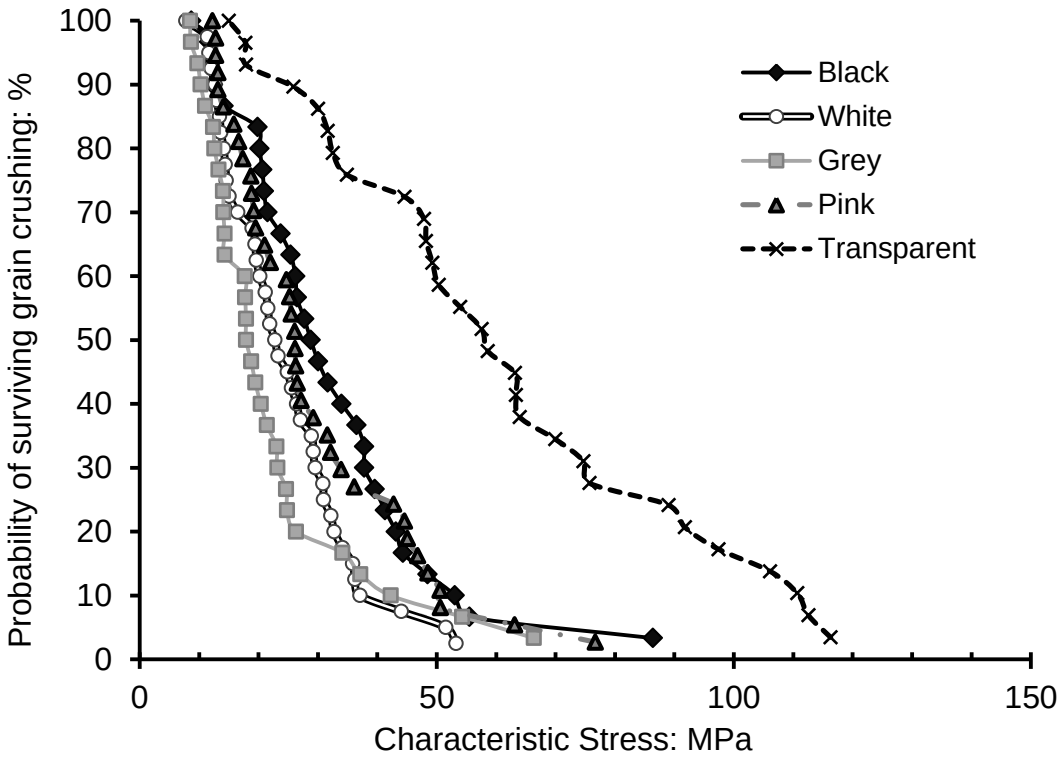

Figure 15. Survival probabilities for the different fractions of Eglin sand.

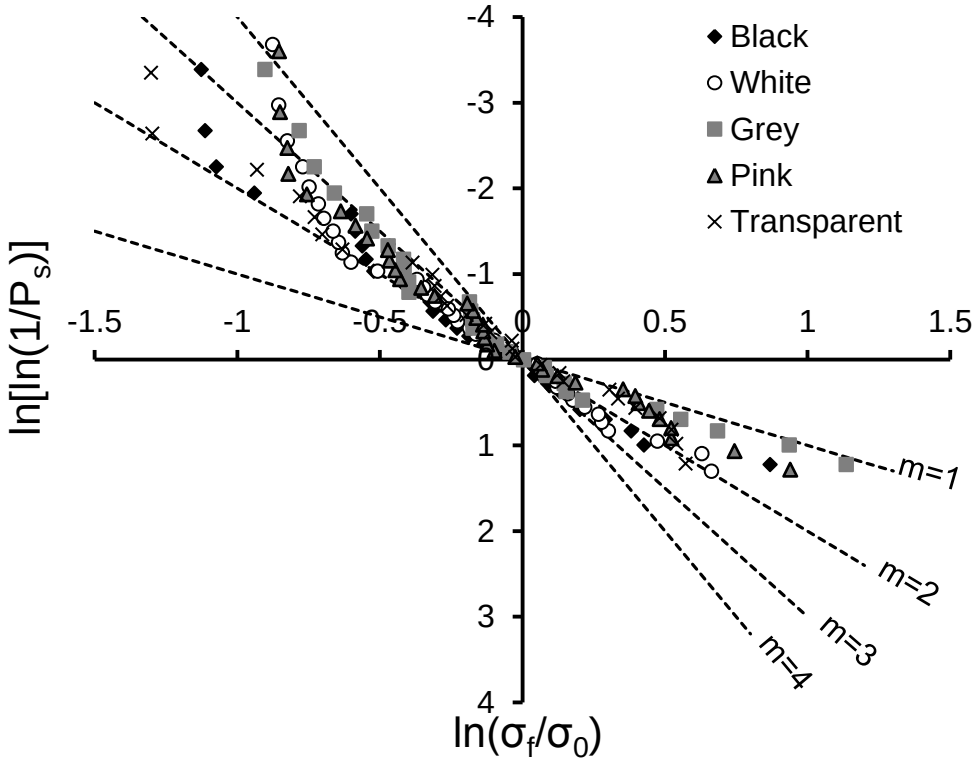

Figure 16. Weibull m-moduli determined for the different fractions of Eglin sand.

TABLES

Table 1. Composition of the fractions of Eglin sand according to their colour.

	Particle Type					
	Black	Grey	Pink	Transparent (feldspar)	Transparent (quartz)	White
Si (%)	35.6	39.7	35.4	29.8	45.5	32.6
O (%)	41.4	49.1	44.1	39.1	53.6	42.76
Al (%)	5.5	3.2	8.4	14.0	0.9	11.6
Fe (%)	7.9	4.6	2.2	1.5	-	1.2
K (%)	0.8	0.3	1.4	9.6	-	8.2
Na (%)	0.6	0.8	5.4	-	-	3.7
Mg (%)	2.6	0.7	0.6	-	-	-
F (%)	2.4	1.5	1.8	-	-	-
Ca (%)	2.6	-	0.3	-	-	-
Mn (%)	0.4	-	-	-	-	-
Ti (%)	-	-	0.3	-	-	-

Table 2. Characteristics of the Eglin sand particles tested.

Particle Type	Average diameter (mm)	Sphericity	Roundness	S_q Roughness (μm)
Black	1.40	0.5	0.4	0.54±0.07
Grey	1.17	0.7	0.5	0.76*
Pink	1.34	0.6	0.5	0.28±0.16
Transparent	1.52	0.8	0.4	0.59±0.07
White	1.55	0.6	0.4	0.69±0.12

*: S_q roundness measured over an area of 16x16μm.

Graphical abstract

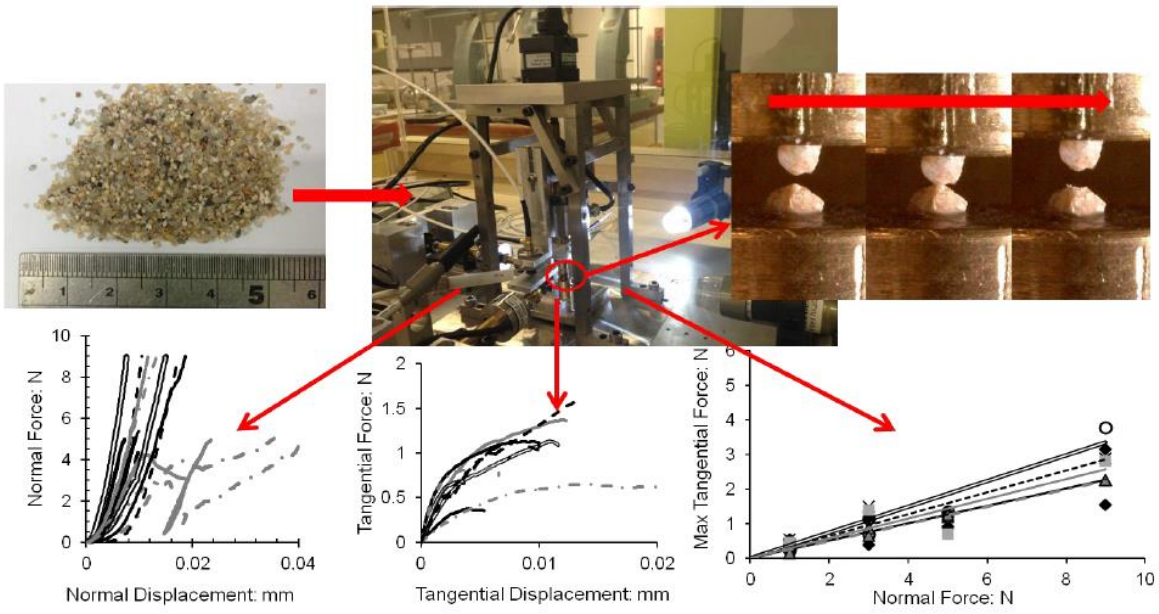

Highlights

- Different particles types were identified within the sample using EDS analyses.
- The normal loading tests can be fitted by the Hertz' theoretical model.
- The shear tests show some scatter in terms of stiffness and friction coefficient.
- The average angles of inter-particle friction vary between 14.0° and 20.4°.
- The particle crushing test results show consistent failure stresses.